INTERNATIONAL JOURNAL FOR NUMERICAL METHODS IN FLUIDS
Int. J. Numer. Meth. Fluids 2002; **40**:1009–1018 (DOI: 10.1002/fld.387)

Unsteady natural convection in tall side-heated cavities

S. Armfield*,† and A. Schultz

Department of Mechanical Engineering, Sydney University, Sydney 2006, Australia

SUMMARY

A finite-volume scheme is used to simulate super-critical natural convection flow in a side-heated cavity with height/width aspect ratio of eight. The flow is unsteady with travelling waves circulating around the cavity in the flow direction. Results on a range of grids with QUICK and central difference advection discretizations show that a very fine grid is required to ensure a converged solution is obtained. A linear parallel stability analysis has been carried out and it is shown that the basic wave structure of the flow is well predicted. Copyright © 2002 John Wiley & Sons, Ltd.

KEY WORDS: unsteady natural convection; finite-volume; QUICK

1. INTRODUCTION

The domain, boundary conditions and governing equations used are those given in Christon *et al.* [1]. A fractional step finite-volume discretization of the Navier–Stokes plus temperature equation on a non-staggered grid has been used, with the equations integrated in time using a Crank–Nicolson discretization for the diffusive terms and Adams–Bashforth for the advective terms. At each time step the temperature and momentum equations are integrated once, using the previous time-step pressure in the momentum equations, to obtain an intermediate velocity field that may not be divergence free. A Poisson equation, with the divergence of the intermediate velocity field as the source term, is then solved to obtain a pressure correction which is used to project the intermediate velocity field onto a divergence free field, and to update the pressure, completing one time step. The advective terms are discretized using either QUICK third-order upwinding [2] or second-order central differencing, all other spatial terms use second-order central differencing. The basic scheme has been previously used for the simulation of natural convection flow [3, 4], as well as other buoyancy-dominated flows [5]. The discretized temperature and momentum equations are inverted using four sweeps of an ADI scheme, while the Poisson pressure correction equation is inverted using a restarted GMRES method. The solution of the pressure correction equation is halted when the integral over the domain of the absolute divergence of the corrected velocity field is less than 1.0×10^{-6}.

* Correspondence to: S. Armfield, School of Aerospace, Mechanical and Mechatronic Engineering, J07, The University of Sydney, Sydney, NSW 2006, Australia.
† E-mail: armfield@aeromech.usyd.edu.au

Received 31 December 2001
Revised 1 July 2002

Table I. Grid details.

Grid		$\Delta x, \Delta y$ at wall	Stretching	Δt	CPUs/time step
G1	35×75	0.02, 0.04	1.07	0.01	0.06
G2	69×155	0.01, 0.02	1.035	0.005	0.33
G3	141×335	0.005, 0.01	1.0175	0.0025	3.5
G4	293×669	0.0025, 0.005	1.00875	0.00125	13.4

Results have been obtained on a range of grids and it is shown that both QUICK and central difference advection schemes converge on a fine enough grid. Additionally, a linear parallel stability analysis has been carried out using the numerical solution as a base flow and it is shown that the basic wave-like features of the flow are well predicted.

2. RESULTS

Results have been obtained for $Ra = 3.4 \times 10^5$ and $Pr = 0.71$ on four grids. Details of the grids, stretching, time step and CPU seconds per time step are shown in Table I. All cases were run on a Compaq Alphaserver DS10 with 466 MHz alpha 21264 processor and 1 Gbyte of memory. For each of the grids the smallest mesh is located adjacent to the solid boundaries, and the mesh is stretched away from the boundary with the stretching shown. The stretching factor is then progressively reduced giving a uniform grid in the interior of the domain. Finer grids are obtained by successively reducing the boundary mesh size and stretching factor by half.

The flow is initialized with a zero velocity and temperature. At time $t = 0$ the left and right walls are impulsively heated and cooled to temperatures of 0.5 and -0.5, respectively, and the flow allowed to develop. It was found that by time $t = 500$ the start-up transients have decayed and the time series shows an oscillatory signal similar to that observed in Le'Quere and DeRoquefort [6]. To obtain the compulsory data for each of the grids the code was run initially to a non-dimensional time of $t = 1000$. The data were then collected over 65536 time steps.

Figure 1 contains results obtained with the QUICK scheme for the G2, G3 and G4 grids. The G2 grid shows only a steady result, with no oscillation, while the G3 and G4 grids both produce a sinusoidal oscillation with nearly identical period, but with the G4 result having the largest amplitude. Figure 2 contains the equivalent results obtained with the central difference scheme. For the central difference scheme all the grids produce a sinusoidal signal, and all grid results are shown. There is a considerable variation in both period and amplitude between the G1 and G2 grid results; however, the G2, G3 and G4 results all show basically the same behaviour, with the G4 result having the largest amplitude. Figures 3 and 4 show a direct comparison of the QUICK and central differencing results on the G3 and G4 grids. Some variation is seen on the G3 grid, with the QUICK scheme giving a smaller amplitude than the central scheme. On the G4 grid both schemes give identical results.

The compulsory data for the X-velocity and temperature average, amplitude and period at point 1, together with the pressure difference at points 1 and 4, and the Nusselt number on the heated wall, are shown in Table II, showing both the grid convergence and the most accurate solution obtained. Only the results obtained with the central difference advection scheme are

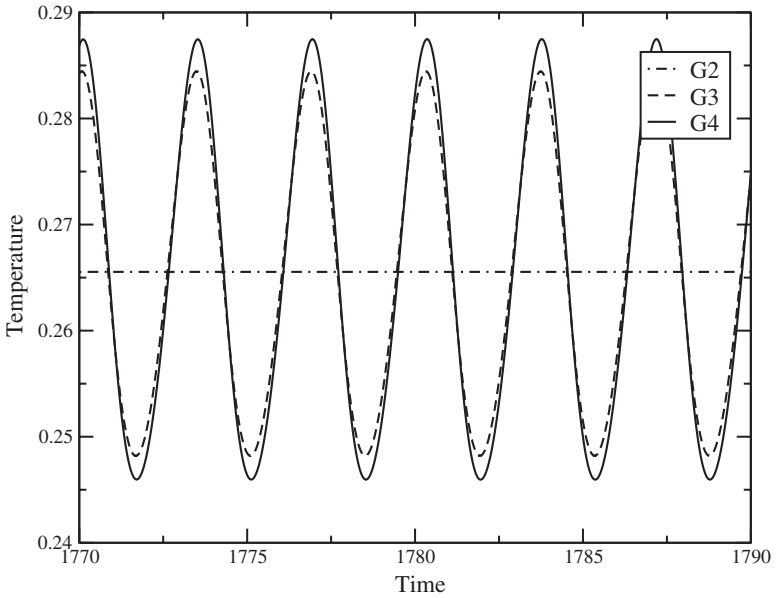

Figure 1. Temperature time series obtained at point 1 with the QUICK scheme.

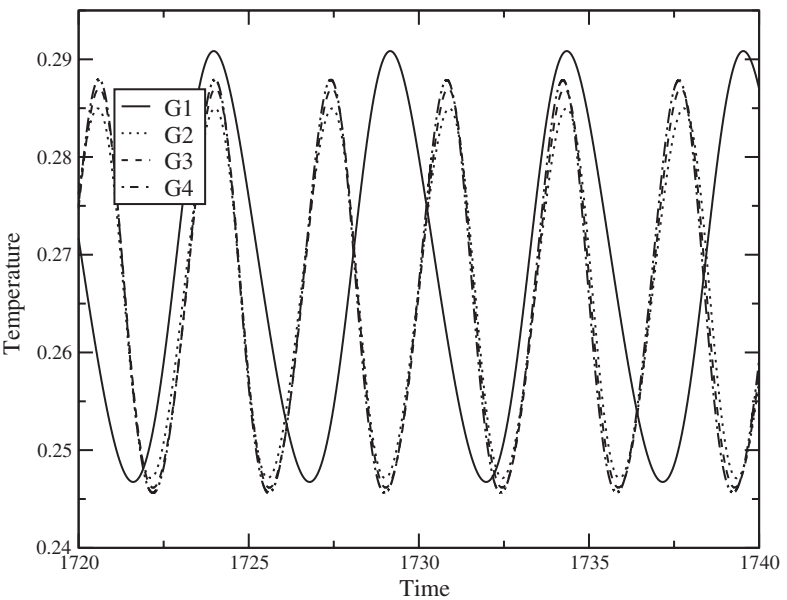

Figure 2. Temperature time series obtained at point 1 with the central scheme.

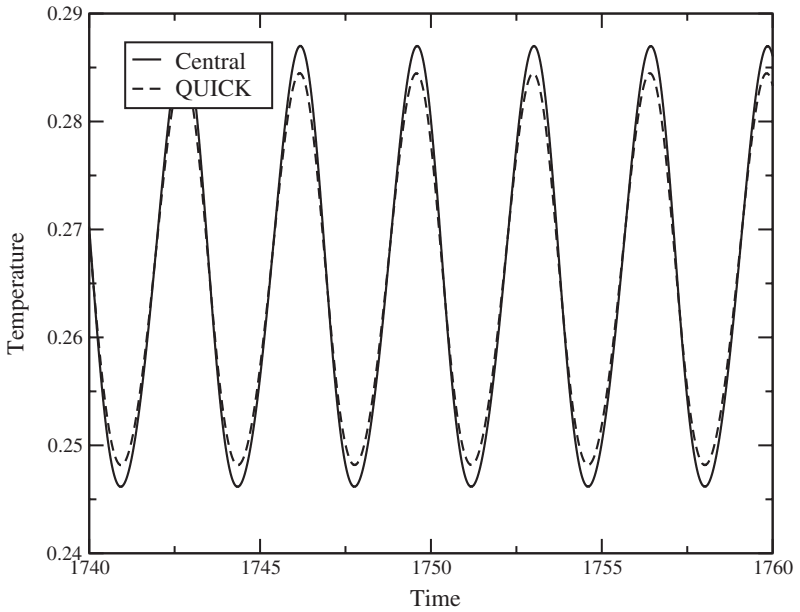

Figure 3. Temperature time series at point 1 with QUICK and central on G3.

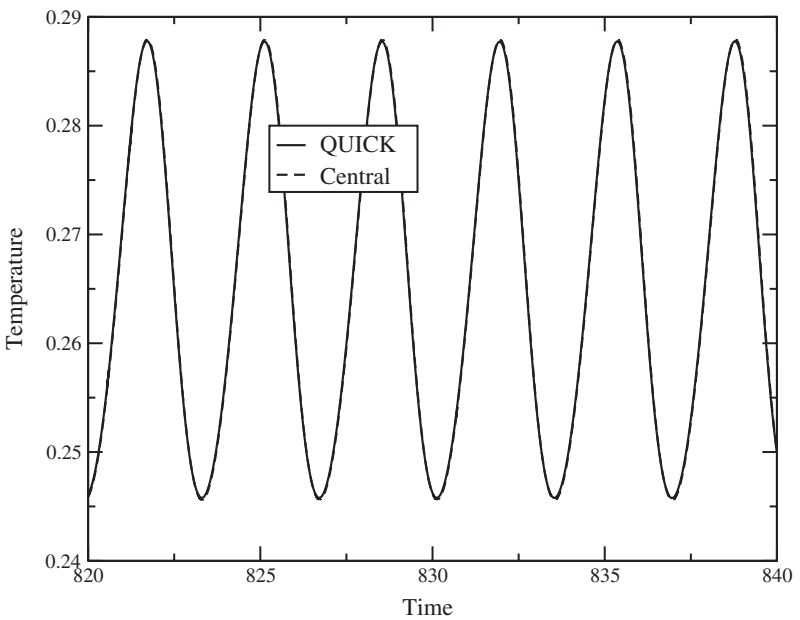

Figure 4. Temperature time series at point 1 with QUICK and central on G4.

Table II. Data obtained with the central difference scheme on the G2, G3 and G4 grids.

	G2: 69×155 Time duration: 328 Steps per period: 340		G3: 141×355 Time duration: 164 Steps per period: 680		G4: 293×699 Time duration: 82 Steps per period: 1360	
Quantity	Average	Amplitude	Average	Amplitude	Average	Amplitude
X-velocity	5.499d-2	4.820d-2	5.608d-2	5.230d-2	5.638d-2	5.382d-2
temperature	2.656d-l	3.784d-2	2.656d-l	4.082d-2	2.656d-l	4.198d-2
ΔP_{14}	1.890d-3	1.806d-2	1.877d-3	1.951d-2	1.855d-3	2.006d-2
Nusselt ($x=0$)	−4.589	6.470d-3	−4.582	6.794d-3	−4.580	6.900d-3
Period	3.4444		3.4191		3.4125	

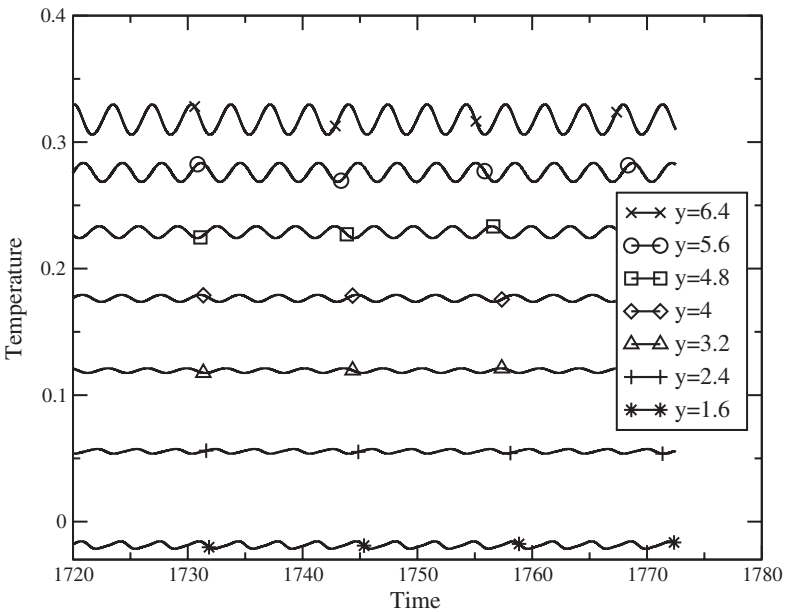

Figure 5. Temperature time series at $x=0.09$.

shown, although it is clear that the QUICK scheme will give very similar values on the G4 grid.

2.1. Stability

The oscillatory signal seen in the temperature time series, shown above, is a result of waves that circulate around the cavity travelling in the flow direction [6]. The waves travel up the heated wall boundary layer, across the horizontal flow region below the upper boundary, down the cooled wall boundary layer, returning to the lower part of the heated wall boundary layer via the horizontal flow region above the bottom boundary. The behaviour of the vertically travelling waves in the vertical boundary layer is shown in Figure 5, where temperature time series obtained at a range of vertical locations within the boundary layer, adjacent to the

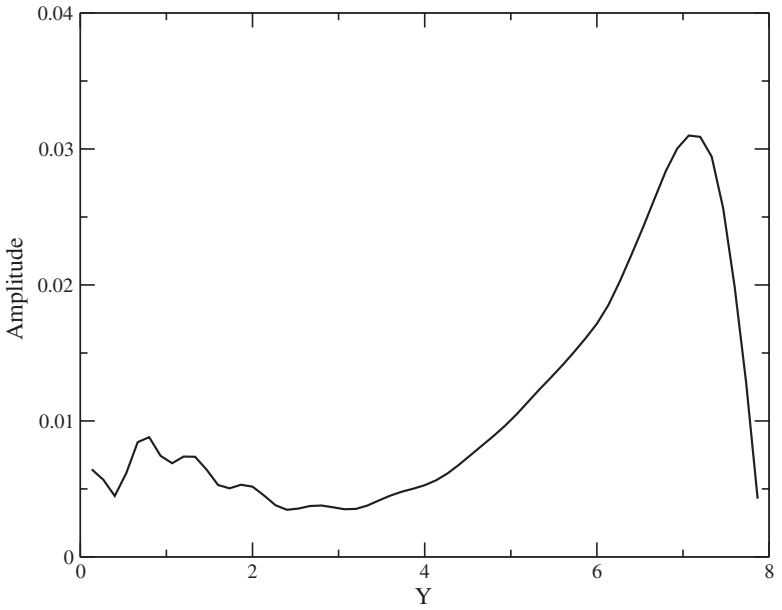

Figure 6. Amplitude of temperature time series at $x=0.09$.

Table III. Wave parameters from simulation at $y=4$.

Amplification ($y=4$)	0.43
Phase velocity ($y=4$)	0.6
Maximum fluid velocity ($y=4$)	0.78
Frequency	0.293
Critical y	$\sim$2.8

heated wall, are shown. The wave structure is seen at all heights in the boundary layer; however, it is also apparent that in the lower part of the boundary layer the waves initially decay, with the smallest amplitude seen at the $y=3.2$ location. Above this location the waves amplify, with the largest amplitude seen at the $y=6.4$ location, the highest location shown. The travelling waves originating at the base of the heated wall boundary layer are therefore seen to initially decay as they travel up the boundary layer, reaching a minimum amplitude at a critical height, then amplifying as they continue to travel above this height. This behaviour is shown in Figure 6, where the amplitude of the travelling waves is plotted against height in the boundary layer. The initial decay and subsequent growth of the waves is clearly seen, while additionally it is observed that the amplitude itself has a wave structure in the lower region of the boundary layer, and the amplitude drops off rapidly above a height of approximately $y=7.0$. Based on the amplitude variation the stability character of the thermal boundary layer may be parameterized in terms of the growth rate of the waves, the phase velocity and the frequency. These quantities at location $y=4$, half the cavity height, are shown in Table III, together with the maximum fluid velocity at this location, which shows that the travelling

waves velocity is slightly less than that of the fluid. Also shown is the critical y location at which the travelling waves change from decay to growth.

It is of interest to determine if the stability character of the boundary layer, as parameterized by the quantities given above, is predicted by a linear parallel stability analysis, providing insight into the basic generation mechanisms associated with the unsteady flow. A stability analysis may be carried out by solving the eigenvalue equations obtained by representing the flow in terms of a base flow plus a perturbation, where the perturbation is of the form

$$\psi = \Re(\psi(x)e^{i\alpha y}e^{i\omega t})$$

$$\tau = \Re(\tau(x)e^{i\alpha y}e^{i\omega t})$$

for the stream function ψ and temperature τ. In this case α is complex with the imaginary component the amplification, and ω is the real temporal wave number, which is related to the frequency by

$$f = \frac{\omega}{2\pi}$$

Substituting these quantities into the governing equations and eliminating non-parallel and non-linear terms give a set of eigenvalue equations in terms of the base flow. The base flow quantities are obtained directly from the numerical simulation and the resulting eigenvalue problem is solved at each vertical location in the cavity, providing a relation between the frequency, amplification and phase velocity at each height [4].

Amplification contours on an ω, y graph are shown in Figure 7, with the thick contour representing the zero amplification curve. Solutions with ω, y values outside the neutral curve are stable, while those inside it are unstable. It is clear that for small y all ω values are stable; however at $y=1.7$ a single ω initially transits the neutral curve, becoming unstable, with a value of approximately $\omega=2.5$. At higher y locations a range of wave numbers are unstable. At $y=4.0$ the unstable range is $1.0<\omega<6.0$, with the maximum amplification occurring at approximately $\omega=4.0$.

Figure 8 shows contours of the phase velocity on an ω, y graph, where it is seen that the boundary layer supports vertically travelling waves with a range of velocities up to slightly greater than 0.55. The stability analysis therefore shows that the thermal boundary layer will support vertically travelling waves with, above a critical height, a band of wave numbers unstable and therefore corresponding to waves that increase in amplitude as they travel. The amplification and phase velocity for the frequency $f=0.293$ predicted by the stability analysis at the half cavity height may be obtained from the amplification and phase velocity plots and compared to that obtained in the simulation, shown in Table III. The frequency $f=0.293$ corresponds to a wave number $\omega=1.84$. The stability and simulation results are compared in Table IV, where it is seen that they are in good agreement, demonstrating that the travelling wave observed at the half-cavity height location is a linear wave resulting from the instability of the locally parallel base flow.

The critical height for the transition to unstable flow obtained from the stability analysis is also compared to that obtained from the simulation in Table IV. The agreement is clearly not as good as that obtained for the quantities at the half-height location.

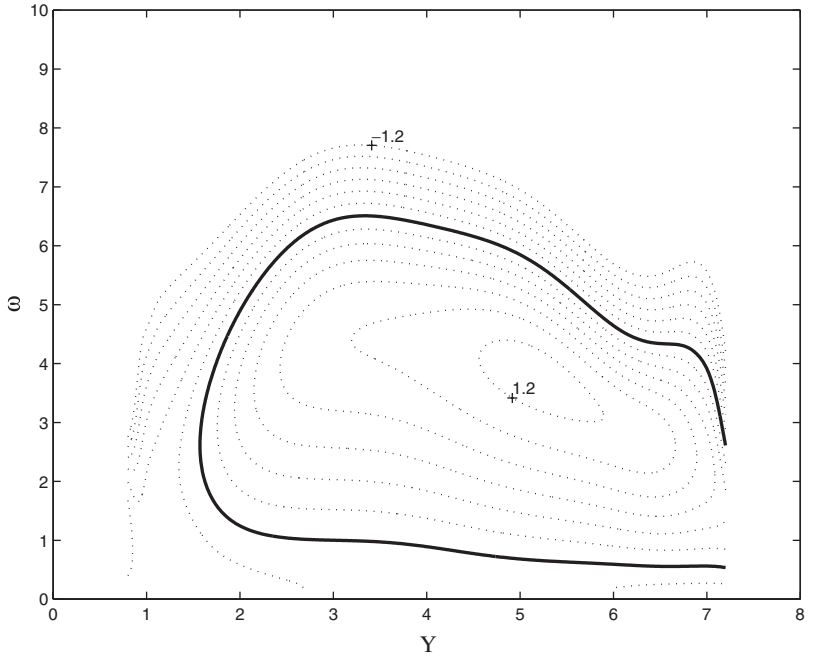

Figure 7. Amplification contours.

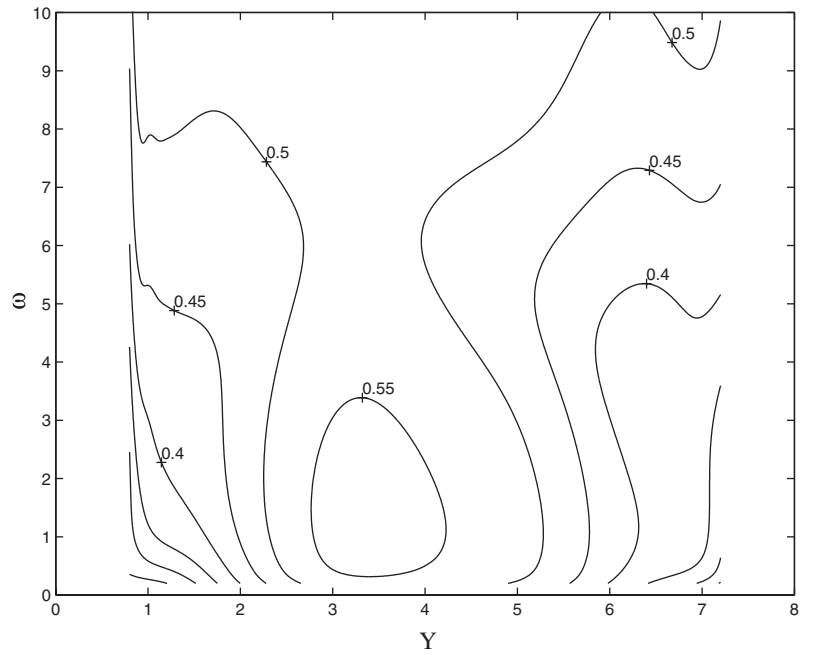

Figure 8. Phase speed contours.

Table IV. Wave parameters from simulation and stability analysis.

	Simulation	Stability ($f=0.293$)
Amplification ($y=4$)	0.43	0.43
Phase velocity ($y=4$)	0.60	0.56
Critical y	$\sim$2.8	1.7

3. DISCUSSION AND CONCLUSIONS

The fractional step projection method used for the solution of the unsteady Navier–Stokes equations is able to produce oscillatory travelling wave solutions in the vertical natural convection cavity flow for the configuration and control parameters specified. Solutions have been obtained for both QUICK and central difference discretizations of the advective terms, and it is clear that both schemes converge to the same solution on the finest grid used. However, considerable variation is seen on the coarser grids. On the G1 and G2 grids the QUICK scheme showed no oscillations, and it is clear that the third-order dissipation inherent in this scheme is damping the instability that leads to the travelling waves. The central scheme, however, showed oscillatory behaviour on all grids, although the solution on G1 is clearly very inaccurate with convergent behaviour only seen on the G2, G3 and G4 grids. Comparing the QUICK and central schemes on G3 it is seen that the central scheme predicts the amplitude more accurately, but the QUICK scheme predicts the period more accurately. The more accurate prediction of the period for the QUICK scheme is a result of that scheme having a higher order dispersion error than that of the central scheme. Finally, it is clear that using an overall second-order scheme of this type it is not possible to obtain significantly more accurate results. The G4 grid result took 135 days of wall clock time to run on the Compaq DS10. A further grid refinement to a G5 grid would require 3 years of wall clock time, which is not feasible. Any additional improvement in accuracy would require a very substantial improvement in computer performance, or the use of a higher order scheme.

It has been hypothesized that the unsteady nature of this flow is a result of a bifurcation that is associated with the stability character of the thermal boundary layers. To test this hypothesis a linear parallel stability analysis was carried out using the numerical simulation as the base flow. The stability analysis showed that the thermal boundary layers support travelling wave solutions, with the lower part of the boundary layer stable and the upper part unstable. Thus on the heated plate boundary layer the flow is convectively unstable above $y=1.7$, and applying a perturbation within the unstable wave number band above this height will lead to travelling waves amplifying as they travel. The stability analysis provided a good prediction of the observed behaviour of the travelling wave at the half-height location in the numerical simulation; however, it underpredicted the location of the critical point at which the flow becomes unstable. It is likely that the underlying assumption of parallel flow is incorrect in the regions of the boundary layer away from the half-height, and this led to the poorer prediction of the critical height.

The stability analysis shows that the boundary layers, above the critical height on the heated wall boundary layer and below the conjugate height on the cooled wall boundary layer, are unstable to a range of wave numbers. However, the simulation clearly shows only a single wave number component. The component observed is that which is unstable in a complete

circuit of the cavity. Even though other wave numbers are unstable in the upper part of the boundary layer, evidently the decay that occurs in the lower part of the boundary layer, in the non-parallel regions adjacent to the upper and lower boundaries, and in the horizontal flow regions, is such that in a single circuit these other wave numbers are stable. If the stability of the wave in a single circuit were entirely governed by that of the boundary layer, and assuming that the linear parallel stability analysis provided a good prediction of the stability properties over the entire height of the boundary layer, the critical wave number observed in the simulation could be predicted by obtaining the wave number with the largest amplification when integrated in the y direction in Figure 7. Inspection of Figure 7 shows that this will be approximately $\omega = 3.0$, which gives a frequency of 0.47 considerably greater than that observed in the simulation. It is therefore clear that the non-parallel boundary layer regions and the horizontal flow regions must contribute more decay to the higher wave number components than is predicted by the linear parallel analysis carried out here, and thus an accurate prediction of the bifurcation frequency would require those regions and effects to be accounted for. However, despite the inability of the linear parallel stability analysis to accurately predict the bifurcation frequency, it does clearly demonstrate that the basic features of the travelling waves are determined by the stability of the thermal boundary layers.

REFERENCES

1. Christon MA, Gresho PM, Sutton SB. Computational predictability of natural convection flows in enclosures. *International Journal for Numerical Methods in Fluids* 2002; **40**:953–980.
2. Leonard BP. A stable and accurate, convective modelling procedure based on quadratic upstream interpolation. *Computer Methods in Applied Mechanics and Engineering* 1979; **19**:59–98.
3. Armfield SW, Patterson JC. Direct simulation of wave interactions in unsteady natural convection in a cavity. *Journal of Fluid Mechanics* 1992; **239**:195–211.
4. Armfield SW, Janssen R. A direct boundary-layer stability analysis of steady-state cavity convection flow. *International Journal of Heat and Fluid Flow* 1996; **17**:539–546.
5. Lin W, Armfield SW. Direct simulation of weak axisymmetric fountains in a homogeneous fluid. *Journal of Fluid Mechanics* 2000; **403**:67–88.
6. Lé Quéré P, DeRoquefort A. Transition to unsteady natural convection of air in vertical differentially heated cavities. In *4th International Conference on Numerical Methods in Laminar and Turbulent Flow*, Swansea. Taylor C (ed.). Pineridge Press: Swansea, 1985; 841–852.

